Extended operating region of modular multilevel converters using full-bridge sub-modules

Extended operating region of modular multilevel converters using full-bridge sub-modules

Ygor Pereira Marca, Jorge L. Duarte, Maurice G. L. Roes and Korneel G. E. Wijnands
Eindhoven University of Technology
Electromechanics and Power Electronics Group
P.O. Box 513, 5600MB
Eindhoven, The Netherlands
Phone: +31 (0) 61-377-4267
Email: y.pereira.marca@tue.nl

Acknowledgments

The authors would like to thank the NEON (New Energy and mobility Outlook for the Netherlands) research team and partners for their support and helpful suggestions.

Keywords

≪Battery≫, ≪Charger≫, ≪Full-bridge≫, ≪Medium-voltage grid≫, ≪Modular multilevel converter≫.

Abstract

This paper presents an application of modular multilevel converters to remove line-frequency transformers from ultrafast charging stations, reducing cost and volume. The converter analysis with full-bridge sub-modules enables an operating region that converts a medium-voltage grid into a lower voltage DC-bus, ideal for charging batteries rapidly.

Introduction

Due to the required power levels of 500kW and above, ultrafast charging stations for large transportation commonly require a connection to the medium-voltage (MV) grid to charge electric vehicle (EV) batteries. Most applications use a line-frequency (LF) step-down transformer (Fig. 1a) to provide isolation and lower the voltage [1]. However, it is convenient to apply instead medium-frequency transformers because it may lead to substantial volume reduction.

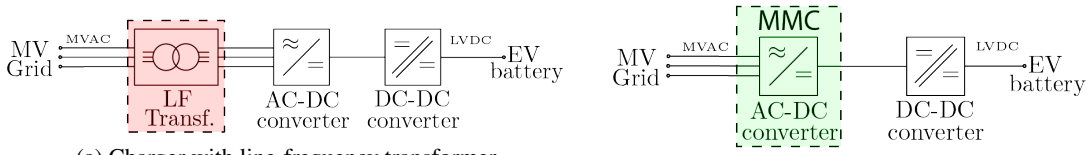

(a) Charger with line-frequency transformer.

(b) Proposed charger.

Fig. 1: Ultrafast charging station architectures.

High-power chargers are an enabling technology for electric transport. In many publications related to [2, 3], it is proposed to replace the line-frequency transformer with cascaded H-bridge converters. Another alternative, the modular multilevel converter (MMC) has been widely implemented in high-voltage direct current (HVDC) systems [4–7], but it is also suitable in MV applications. Although it can connect a MV grid to a lower DC-bus voltage, MMCs are normally employed to generate a high-voltage DC-bus, requiring many input-series and output-parallel DC-DC converters with medium-frequency transformers

to step-down the voltage for battery connection and isolation purposes [8]. Therefore, this paper explores the possibilities and challenges of using a MMC to interface a MV grid and to a lower voltage DC-bus (Fig. 1b), so that the isolation stage can be designed for a lower voltage and optimized for a fixed voltage ratio, enabling soft-switching over the entire operating range [9].

Modular multilevel converter

Proposed in 2002 [10], the MMC (Fig.2) is generally applied for high-voltage and high-power conversion, because of its modularity, output voltage quality, and high efficiency. Its configuration is scalable to different voltage and power requirements. Moreover, the voltage across semiconductors is reduced since sub-modules (SMs) are connected in series, and its modularity allows redundancy [11].

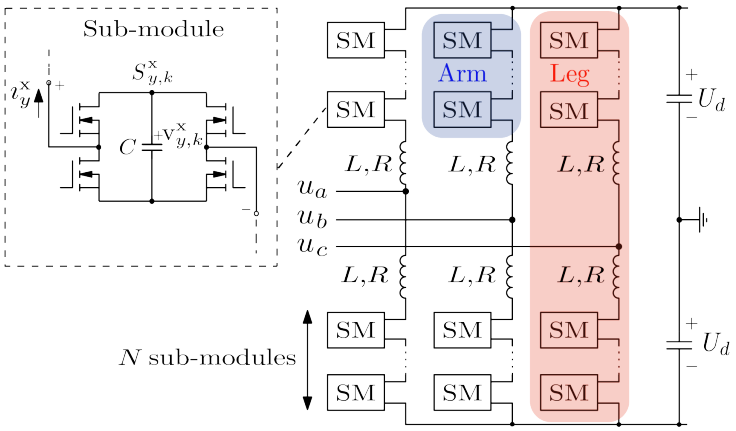

Fig. 2: Three-phase modular multilevel converter with full-bridge sub-modules.

As can be seen in Fig. 2, each converter phase leg has two arms: a lower and an upper arm. The arms have a number (N) of series-connected SMs, which consist of a full-bridge (FB) converter with a capacitor. While an MMC based on half-bridge (HB) SMs can only generate a DC-bus voltage higher than the maximum rectified value, a converter based on FB SMs can provide a DC-bus voltage lower than the AC voltage amplitude [12].

Fundamentals

The FB SMs can be represented as controllable voltage sources [11]. Therefore, to simplify the converter analysis, these voltage sources are used instead of switches and capacitors. Furthermore, since the three legs operate identically, the analysis will be performed for a single-phase.

Full-bridge sub-modules

As the converter may have many sub-modules, it is desirable to simplify the analysis using convenient definitions. The k^{th} sub-modules' switching function is represented by $S^{x}_{y,k} \in \{-1,0,1\}$, with arms represented by $x \in \{u,\ell\}$ and grid phase expressed as $y \in \{a,b,c\}$.

The currents that flow in the equivalent circuit of a single-phase MMC, presented in Fig. 3, are the upper ($\imath^{u}_{y}$) and lower ($\imath^{\ell}_{y}$) arm currents, and grid current ($\imath_y$). In addition, the voltage sources in the circuit are denominated as the upper (u^{u}_{y}) and lower (u^{ℓ}_{y}) arm voltages, together with grid (u_y) and the DC-bus (U_d) voltage.

Applying Kirchhoff's Voltage Law in the upper and lower loop in Fig. 3 results in

$$L\frac{d}{dt}\imath^{u}_{y} + R\imath^{u}_{y} = u^{u}_{y} + u_y - U_d, \qquad (1)$$

$$L\frac{d}{dt}\imath^{\ell}_{y} + R\imath^{\ell}_{y} = u^{\ell}_{y} - u_y - U_d. \qquad (2)$$

For the purpose of analysis it is convenient to split the circulating arm currents into components, namely, common-mode current ($\imath^{\Sigma}_{y}$) and differential-mode current ($\imath^{\Delta}_{y}$), as

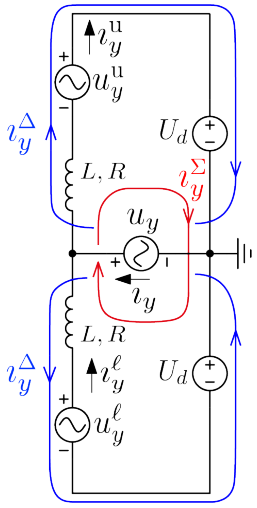

Fig. 3: Equivalent circuit of the single-phase FB MMC.

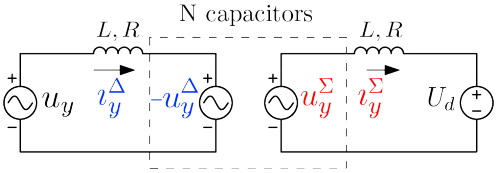

Fig. 4: Decoupled model of the single-phase FB MMC.

$$i_y^{\Sigma} = \frac{1}{2}\left(i_y^{\mathrm{u}} + i_y^{\ell}\right), \tag{3}$$

$$i_y^{\Delta} = \frac{1}{2}\left(i_y^{\mathrm{u}} - i_y^{\ell}\right). \tag{4}$$

Similarly, it is also favorable to split the arm voltages into common-mode voltage (u_y^{Σ}) and differential-mode voltage (u_y^{Δ}), as

$$u_y^{\Sigma} = \frac{1}{2}\left(u_y^{\mathrm{u}} + u_y^{\ell}\right), \tag{5}$$

$$u_y^{\Delta} = \frac{1}{2}\left(u_y^{\mathrm{u}} - u_y^{\ell}\right). \tag{6}$$

Many MMC analyses are performed using HB SMs [11, 13]. In this paper, the dynamic analysis of the MMC will be evaluated using FB SMs. Therefore, adding and subtracting (1) and (2), and substituting (4), (3), (6), and (5) yields

$$L\frac{d}{dt}i_y^{\Sigma} + Ri_y^{\Sigma} = u_y^{\Sigma} - U_d, \tag{7}$$

$$L\frac{d}{dt}i_y^{\Delta} + Ri_y^{\Delta} = u_y^{\Delta} + u_y. \tag{8}$$

With (7) and (8), it is possible to describe an equivalent circuit model for the FB modular multilevel converter as exhibited in Fig. 4, which shows that the controllable voltage sources used to control the operation of a MMC arm, have an AC ($-u_y^{\Delta}$), and a DC (u_y^{Σ}) component, resulting in a decoupled model description.

The voltages across the MMC arms u_y^{u} and u_y^{ℓ} are the sum of both voltage components, as presented in Fig. 5. The ripple voltage in u_y^{Σ} is small in comparison with the DC and AC voltages, so it has a low influence on the arm voltage waveform. The upper arm voltage in Fig. 5 shows the MMC in the operating region c (Fig. 6), which can be performed by both HB and FB SMs.

The operating region in which the grid voltage amplitude ($\widehat{U}_y \approx \widehat{U}_y^{\Delta}$) is higher than the DC-bus voltage (U_d) is highlighted by triangle b (Fig. 6). So, region b is an advantage of using FBs instead of HBs in MMC sub-modules because it allows the connection of a MV grid with a lower voltage DC-bus. In addition, the operating regions presented by triangles a and c in Fig. 6 are commonly used to operate the MMC during DC-side faults and to produce a high-voltade DC-bus, respectively [14, 15]. Note that the total capacitor voltage ($\mathrm{v}_y^{\mathrm{x}}$), defined in section , is composed by both U_d and $\widehat{U}_y^{\Delta}$.

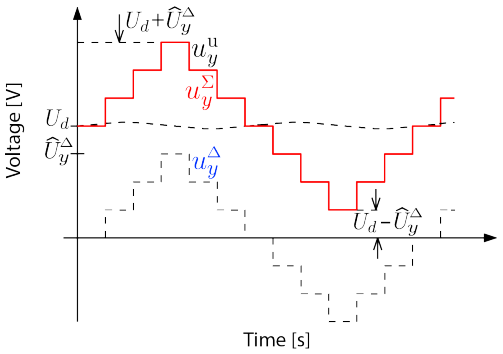

Fig. 5: MMC upper arm voltage (u_y^{u}) and its relation to the differential-mode (u_y^{Δ}) and common-mode (u_y^{Σ}) components.

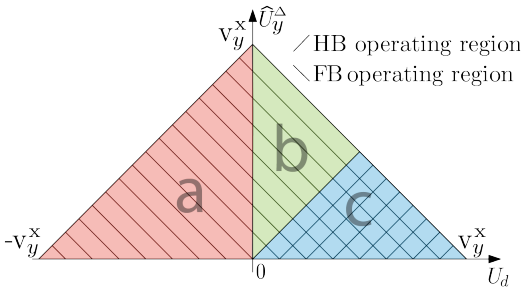

Fig. 6: MMC operating regions with HB and FB SMs.

Arm energy

The stored energy in the sub-modules of each arm is utilized to describe the common-mode and differential-mode energies, which can be used to balance the capacitor voltages [13]. The total capacitor voltage ($\mathrm{v}_y^{\mathrm{x}}$) and total energy ($\mathscr{E}_y^{x}$) are given by

$$\mathrm{v}_y^{\mathrm{x}} = \sum_{k=1}^{N} \mathrm{v}_{y,k}^{\mathrm{x}}, \tag{9}$$

$$\mathscr{E}_y^{x} = \sum_{k=1}^{N} \frac{1}{2} C \left(\mathrm{v}_{y,k}^{\mathrm{x}}\right)^2. \tag{10}$$

The capacitors in each arm are connected in series, and assuming their voltages are balanced, the total capacitor voltage and capacitance of each arm are

$$\mathrm{v}_{y,k-1}^{\mathrm{x}} \approx \mathrm{v}_{y,k}^{\mathrm{x}} \approx \mathrm{v}_{y,k+1}^{\mathrm{x}} \approx \ldots \approx \frac{1}{N} \mathrm{v}_y^{\mathrm{x}}, \tag{11}$$

$$C_\sigma = \frac{C}{N}. \tag{12}$$

Furthermore, the arm voltages and average insertion indexes of the converter can be defined as

$$u_y^{x} = \sum_{k=1}^{N} S_{y,k}^{x} \mathrm{v}_{y,k}^{\mathrm{x}}, \tag{13}$$

$$n_y^{x} = \frac{1}{N} \sum_{k=1}^{N} S_{y,k}^{x}. \tag{14}$$

Thus, the variation of the arm energy and the variation of the capacitors' voltage are given by

$$\frac{d}{dt} \mathscr{E}_y^{x} = C_\sigma \mathrm{v}_y^{\mathrm{x}} \frac{d}{dt} \mathrm{v}_y^{\mathrm{x}}, \tag{15}$$

$$\frac{d}{dt} v_y^{\mathrm{x}} = -\frac{1}{C_\sigma} n_y^{x} i_y^{x}. \tag{16}$$

Energy distribution

As presented in (4), (5), and (6), the energy can be presented in relation to the common-mode ($\mathscr{E}_y^{\Sigma}$) and differential-mode ($\mathscr{E}_y^{\Delta}$) components. In a stable controlled system, the common-mode energy remains constant and the differential-mode energy is zero while operating because it is desirable to have balanced energy to decrease the capacitive energy storage.

$$\mathscr{E}_y^{\Sigma} = \frac{1}{2} \left(\mathscr{E}_y^{\mathrm{u}} + \mathscr{E}_y^{\ell} \right), \tag{17}$$

$$\mathscr{E}_y^{\Delta} = \frac{1}{2} \left(\mathscr{E}_y^{\mathrm{u}} - \mathscr{E}_y^{\ell} \right). \tag{18}$$

Therefore, (17) and (18) can be derived and replaced into (15), and with some algebraic manipulations the variation of the common-mode and differential-mode energies are defined as

$$\frac{d}{dt}\mathscr{E}_y^{\Sigma} = -\left(u_y^{\Sigma} i_y^{\Sigma} + u_y^{\Delta} i_y^{\Delta}\right), \tag{19}$$

$$\frac{d}{dt}\mathscr{E}_y^{\Delta} = -\left(u_y^{\Delta} i_y^{\Sigma} + u_y^{\Sigma} i_y^{\Delta}\right). \tag{20}$$

The equations above are used for energy balancing control of the MMC as presented in [11].

Averaged equivalent circuit

Finally, to simplify the analysis of the converter, it is possible to approximate the behaviour of the MMC using an averaged equivalent circuit [16]. The model is useful to simulate the MMC without modulation and individual capacitor voltage balancing, as shown in Fig. 7.

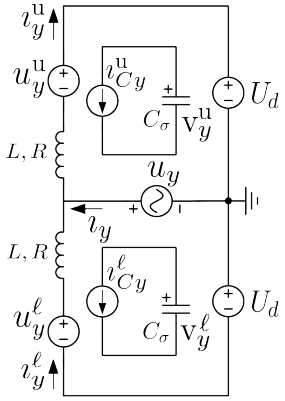

Fig. 7: Averaged equivalent circuit for a single-phase MMC.

Since the capacitor voltages are assumed to be equal for every module in the arm, the arm voltages and capacitor currents can be steered by an average insertion index as

$$u_y^x = n_y^x \mathrm{v}_y^{\mathrm{x}}, \tag{21}$$

$$i_{Cy}^x = -C_\sigma \frac{d}{dt}\mathrm{v}_y^{\mathrm{x}} = n_y^x i_y^x. \tag{22}$$

Efficiency

An estimation of the charger efficiency can be determined by considering first the switch conduction losses. The required minimum number of SMs per arm and a practical maximum voltage level for application purposes are given by

$$N = \left\lceil \frac{\widehat{U}_y + U_d}{\mathrm{V}_{sw}} \right\rceil, \tag{23}$$

$$\mathrm{V}_{sw} = \mathrm{V}_{ds} D_F. \tag{24}$$

where V_{ds} and D_F are the semiconductor device breakdown voltage and derating factor, respectively. Switching losses may be disregarded when considering 1.2kV SiC MOSFETs. The arm current and total conduction losses of the converter are given by

$$I_y^{\mathrm{x}} = \sqrt{\left(I_y^{\Sigma}\right)^2 + \left(I_y^{\Delta}\right)^2}, \tag{25}$$

$$P_{\mathrm{loss}} = 4 R_{ds} N (I_y^{\mathrm{x}})^2. \tag{26}$$

With (26), the power efficiency can be estimated on the basis of the nominal processed power.

Simulation results

Equations (7), (8), (19), (20), (21) and (22) allow to control the MMC such that a lower voltage output can be derived directly from a MV grid based in [11]. Thus, simulations were conducted with the main circuit parameters described in Table 1. Fig. 8 shows the resulting efficiency as a function of the DC-bus voltage. It is possible to see that above $U_d = 10$ kV, the conduction losses represent less than 1% of the processed power.

Table I: Ratings of the simulated MMC with FB SMs.

Description	Variable	Value	Unit
Rated active power	P	1	MW
AC peak voltage	$\hat{U}_y$	25	kV
Grid frequency	f	50	Hz
Arm capacitance	C_σ	1	mF
Arm inductance	L	3	mH
Arm resistance	R	0.05	Ω
MOSFET breakdown voltage	V_{ds}	1.2	kV
MOSFET derating factor	D_F	75	%
MOSFET on-resistance	R_{ds}	20	mΩ

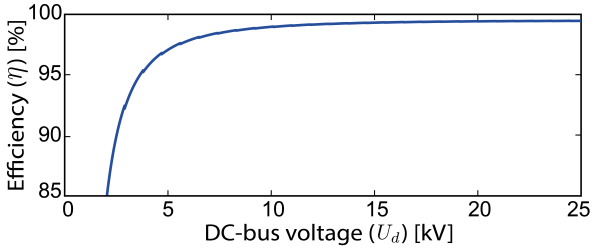

Fig. 8: MMC efficiency in relation to the DC-bus voltage.

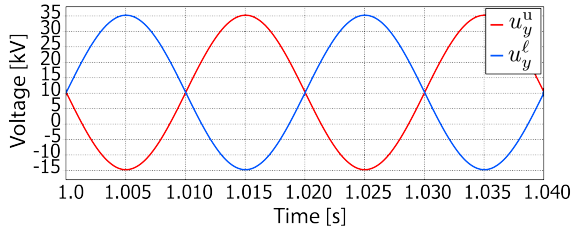

(a) Upper and lower arm voltages.

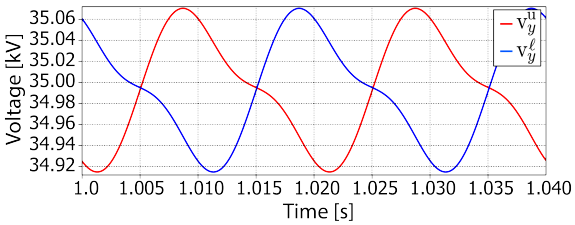

(b) Sum of capacitor voltages in the upper and lower arms.

Fig. 9: Steady-state voltage waveforms.

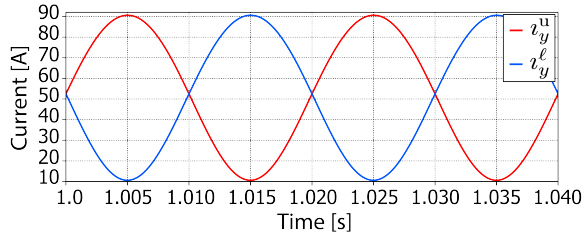

(a) Upper and lower arm currents.

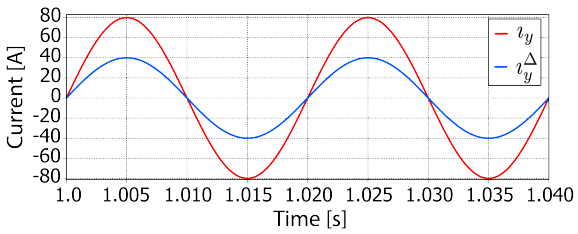

(b) Grid and differential-mode currents.

Fig. 10: Steady-state current waveforms.

The arm voltages presented in Fig. 9a show the offset introduced by the DC-bus voltage of 10 kV and

Fig. 9b illustrates that the total capacitor voltages in both arms are defined by the AC peak voltage and the DC-bus voltage. In addition, Fig. 10a shows the arm currents and Fig. 10b presents the grid and differential-mode currents in accordance with the equivalent circuit in Fig. 3, where $\imath_y = 2\imath_y^{\Delta}$.

Conclusion

Since its first appearance, the MMC has been regularly applied in HVDC. Adopting FB SMs increase the converter's operating region, which allows converting the voltage of a MV grid to a lower voltage directly. This region of operation is useful for high-power battery-to-grid-applications such as the charge and discharge of large electric transportation, presenting itself as an alternative for cascaded H-bridge converters. Therefore, with the presented topology, a downstream DC-DC converter stage optimized for a fixed voltage ratio containing a medium-frequency transformer can provide galvanic isolation.

Simulations show that high efficiency is achieved with a DC-bus voltage lower than the medium-voltage grid. Moreover, the steady-state waveforms corroborate the suitability for high-power bidirectional battery chargers.

References

[1] S. Srdic and S. Lukic, "Toward extreme fast charging: Challenges and opportunities in directly connecting to medium-voltage line," *IEEE Electrification Magazine*, vol. 7, no. 1, pp. 22–31, 2019.

[2] M. Vasiladiotis, A. Rufer, and A. Béguin, "Modular converter architecture for medium voltage ultra fast ev charging stations: Global system considerations," in *2012 IEEE International Electric Vehicle Conference*. IEEE, 2012, pp. 1–7.

[3] M. Awal, I. Husain, M. R. H. Bipu, O. A. Montes, F. Teng, H. Feng, M. Khan, and S. Lukic, "Modular medium voltage ac to low voltage dc converter for extreme fast charging applications," *arXiv preprint arXiv:2007.04369*, 2020.

[4] W. Lin, D. Jovcic, S. Nguefeu, and H. Saad, "Full-bridge mmc converter optimal design to hvdc operational requirements," *IEEE Transactions on Power Delivery*, vol. 31, no. 3, pp. 1342–1350, 2015.

[5] A. Nami, J. Liang, F. Dijkhuizen, and G. D. Demetriades, "Modular multilevel converters for hvdc applications: Review on converter cells and functionalities," *IEEE Transactions on Power Electronics*, vol. 30, no. 1, pp. 18–36, 2014.

[6] S. Allebrod, R. Hamerski, and R. Marquardt, "New transformerless, scalable modular multilevel converters for hvdc-transmission," in *2008 IEEE Power Electronics Specialists Conference*. IEEE, 2008, pp. 174–179.

[7] P. Bakas, Y. Okazaki, A. Shukla, S. K. Patro, K. Ilves, F. Dijkhuizen, and A. Nami, "Review of hybrid multilevel converter topologies utilizing thyristors for hvdc applications," *IEEE Transactions on Power Electronics*, 2020.

[8] Z. Li, P. Wang, Z. Chu, H. Zhu, Z. Sun, and Y. Li, "A three-phase 10 kvac-750 vdc power electronic transformer for smart distribution grid," in *2013 15th European Conference on Power Electronics and Applications (EPE)*. IEEE, 2013, pp. 1–9.

[9] N. H. Baars, J. Everts, C. G. Wijnands, and E. A. Lomonova, "Performance evaluation of a three-phase dual active bridge dc–dc converter with different transformer winding configurations," *IEEE Transactions on Power Electronics*, vol. 31, no. 10, pp. 6814–6823, 2015.

[10] R. Marquardt, A. Lesnicar, J. Hildinger *et al.*, "Modulares stromrichterkonzept für netzkupplungsanwendung bei hohen spannungen," *ETG-Fachtagung, Bad Nauheim, Germany*, vol. 114, 2002.

[11] A. Antonopoulos, L. Angquist, and H.-P. Nee, "On dynamics and voltage control of the modular multilevel converter," in *2009 13th European Conference on Power Electronics and Applications*. IEEE, 2009, pp. 1–10.

[12] K. Sharifabadi, L. Harnefors, H.-P. Nee, S. Norrga, and R. Teodorescu, *Design, control, and application of modular multilevel converters for HVDC transmission systems*. John Wiley & Sons, 2016.

[13] L. Ängquist, A. Antonopoulos, D. Siemaszko, K. Ilves, M. Vasiladiotis, and H.-P. Nee, "Inner control of modular multilevel converters-an approach using open-loop estimation of stored energy," in *The 2010 International Power Electronics Conference-ECCE ASIA-*. IEEE, 2010, pp. 1579–1585.

[14] R. Marquardt, "Modular multilevel converter: An universal concept for hvdc-networks and extended dc-bus-applications," in *The 2010 International Power Electronics Conference-ECCE ASIA-*. IEEE, 2010, pp. 502–507.

[15] G. P. Adam and I. E. Davidson, "Robust and generic control of full-bridge modular multilevel converter high-voltage dc transmission systems," *IEEE Transactions on Power Delivery*, vol. 30, no. 6, pp. 2468–2476, 2015.

[16] D. C. Ludois and G. Venkataramanan, "Simplified terminal behavioral model for a modular multilevel converter," *IEEE Transactions on Power Electronics*, vol. 29, no. 4, pp. 1622–1631, 2013.